Acta Crystallographica Section B
Structural Science
ISSN 0108-7681

Structures of the cation-deficient perovskite $Nd_{0.7}Ti_{0.9}Al_{0.1}O_3$ from high-resolution neutron powder diffraction in combination with group-theoretical analysis

Zhaoming Zhang,[a]* Christopher J. Howard,[a] Kevin S. Knight[b,c] and Gregory R. Lumpkin[a,d]

[a]Australian Nuclear Science and Technology Organisation, Private Mail Bag 1, Menai, NSW 2234, Australia, [b]ISIS Facility, Rutherford Appleton Laboratory, Chilton, Didcot OX11 0QX, England, [c]Department of Mineralogy, The Natural History Museum, Cromwell Road, London SW7 5BD, England, and [d]Department of Earth Sciences, University of Cambridge, Downing Street, Cambridge CB2 3EQ, England

Correspondence e-mail: zzx@ansto.gov.au

Received 19 September 2005
Accepted 8 December 2005

The crystal structures of $Nd_{0.7}Ti_{0.9}Al_{0.1}O_3$, taken to represent the ideal $Nd_{2/3}TiO_3$, have been elucidated from 4 to 1273 K using high-resolution neutron powder diffraction in combination with group-theoretical analysis. The room-temperature structure is monoclinic in $C2/m$, on a cell with a = 7.6764 (1), b = 7.6430 (1), c = 7.7114 (1) Å, β = 90.042 (2)°. Pertinent features are the layered ordering of the A-site Nd cations/vacancies along the z axis and out-of-phase tilting of the (Ti/Al)O_6 octahedra around both the x and z axes. From about 750 to 1273 K, the octahedra are tilted around just one axis (x axis) perpendicular to the direction of the cation ordering, giving rise to an orthorhombic structure with space-group symmetry *Cmmm*.

1. Introduction

The crystal structures and cation/vacancy ordering in perovskite systems with A-site vacancies, $A_x\square_{(1-x)}BO_3$, are of interest for potentially attractive properties of ionic conductivity, dielectric behaviour and magnetic response. Mitchell (2002) surveyed the published structural data for this class of materials and concluded that further studies are required as many of the reported structures are probably incorrect. $Nd_{2/3}TiO_3$ is such a compound with one third of the A sites vacant. The crystal structure of $Nd_{2/3}TiO_3$ was first reported by Yoshii (2000) as orthorhombic in the space group *Pmmm* on a $1 \times 1 \times 2$ cell (referred to the edge of the cubic aristotype). It was suggested by Howard & Zhang (2004*a*,*b*) that $Nd_{2/3}TiO_3$ would be isostructural with $La_{2/3}TiO_3$, which has an orthorhombic structure in *Cmmm* on a $2 \times 2 \times 2$ cell. More recently, Sefat *et al.* (2005) refined the powder neutron data of $Nd_{0.7}TiO_3$ in both *Cmmm* (on a $2 \times 2 \times 2$ cell) and *Pban* (on a $2^{1/2} \times 2^{1/2} \times 2$ cell) and found the *Cmmm* model to be superior. It is generally accepted that $Nd_{2/3}TiO_3$ is unstable in its pure form. However, the structure can be stabilized at a slight oxygen deficiency (Yoshii, 2000) or by low-level doping with $NdTiO_3$ (Sefat *et al.*, 2005) or $NdAlO_3$ (Lee *et al.*, 2004). Lee *et al.* (2004) studied the microstructure of the $(1-x)$-$Nd_{2/3}TiO_3$–$xNdAlO_3$ system using transmission electron microscopy (TEM). They recorded superlattice reflections indicative of cell doubling in one direction for x = 0.1–0.7 and attributed this to different ionic populations on successive layers of the perovskite A-site. They also proposed for $Nd_{0.7}Ti_{0.9}Al_{0.1}O_3$ (x = 0.1) both out-of-phase and in-phase tilting of the oxygen octahedra along with A-site cation displacement, based on the observation of superlattice reflections indexing, when referred to the cell of the aristotype, at $\frac{1}{2}$(*odd odd odd*), $\frac{1}{2}$(*odd odd even*) and $\frac{1}{2}$(*odd even even*). However, no space-group symmetry was assigned to their structures.

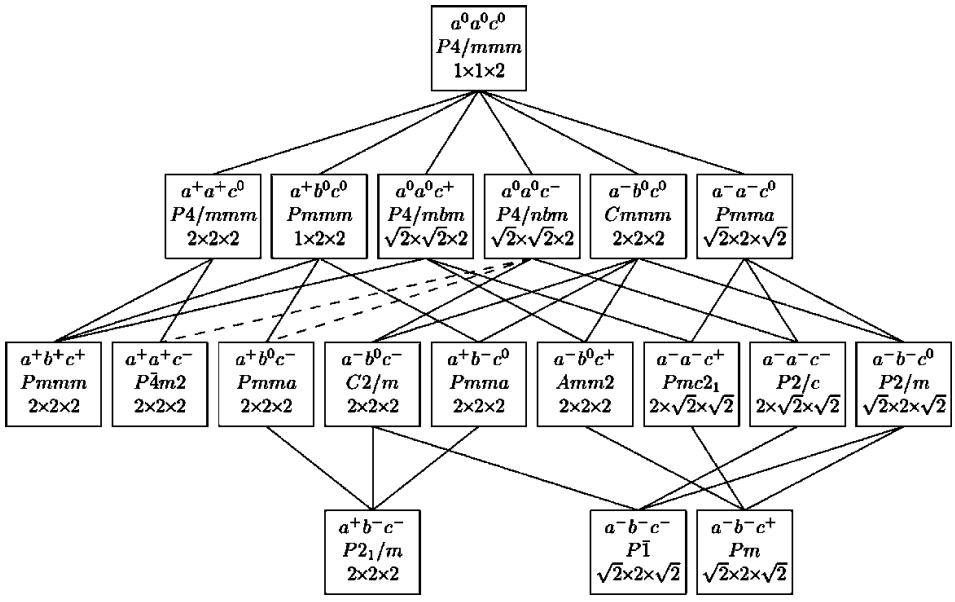

Figure 1
A schematic diagram showing the different possible structures generated by the layered ordering of cations on the perovskite *A* site, followed by the tilting of the corner-linked BX_6 octahedra. The tilting pattern is indicated using Glazer's notation, as explained in the text. The space group is shown, along with the approximate cell dimensions in terms of the cell edge of the $Pm\bar{3}m$ parent – angles not required to be 90° are approximately 90°. The lines on the schematic indicate group–subgroup relationships among the 19 space groups shown – a dashed line indicates that, according to Landau theory, the corresponding phase transition cannot be continuous. This figure has been reproduced from Howard & Stokes (2004).

In this paper, we report a new monoclinic structure for the composition $Nd_{0.7}Ti_{0.9}Al_{0.1}O_3$. The structure has been deduced through a combination of high-resolution neutron powder diffraction and group-theoretical analysis. The structure, in the space group *C2/m* on a $2 \times 2 \times 2$ cell, is characterized by a layered ordering of the *A*-site cations/vacancies, and $(Ti/Al)O_6$ octahedral tilting independently around two axes. Temperature studies of the transition to the orthorhombic structure *Cmmm* are also reported.

2. Symmetry considerations

Among the room-temperature structures considered for $Nd_{2/3}TiO_3$ (Yoshii, 2000; Howard & Zhang, 2004*a*,*b*), $Nd_{0.7}TiO_3$ (Sefat *et al.*, 2005) and $Nd_{0.7}Ti_{0.9}Al_{0.1}O_3$ (Lee *et al.*, 2004), there is a consensus on cell doubling in at least one direction, arising from a layered ordering of Nd such that one layer is rich in the cations, and the next is poorer in cations since it contains a greater number of vacancies. It is also agreed that the room-temperature structure is orthorhombic, however, the detailed driving mechanism for the orthorhombic distortion has been a matter for conjecture. Based on our previous experience, we believe that the room-temperature structure arises from a layered ordering of *A*-site cations/vacancies in combination with the tilting of corner-linked BX_6 octahedral units relative to one another (Howard & Zhang, 2003, 2004*a*,*b*). Again a group-theoretical approach was used to enumerate the possible structures. The methodology has been described at greater length in two recent publications by Howard & Stokes (2004, 2005).

The layered ordering of cations (or vacancies) on the perovskite *A*-site was recognized as transforming according to the irreducible representation X_3^- ($\mathbf{k} = 0,0,\frac{1}{2}$) of the aristotype space group $Pm\bar{3}m$ and giving rise to a structure in the space group *P*4/*mmm* on a $1 \times 1 \times 2$ cell. The octahedral tilting was represented through the irreducible representations (irreps) R_4^+ ($\mathbf{k} = \frac{1}{2},\frac{1}{2},\frac{1}{2}$) corresponding to modes with out-of-phase tilting of octahedra in successive layers and M_3^+ ($\mathbf{k} = \frac{1}{2},\frac{1}{2},0$) associated with in-phase octahedral tilting. The different possible structures were obtained using the computer program *ISOTROPY*,[1] with results as summarized here in Fig. 1. For each structure, that figure shows the space group with the tilt system indicated, described using Glazer's notation (Glazer, 1972, 1975) – briefly, the symbol $a^\#b^\#c^\#$ is used to indicate no tilt, in-phase octahedral tilting or out-of-phase octahedral tilting around the ⟨001⟩ axes of the parent $Pm\bar{3}m$ perovskite by showing the superscript # as 0, + or −, respectively. The figure also includes the approximate dimensions of the unit cell in terms of the cell edge of the $Pm\bar{3}m$ aristotype. The group–subgroup relationships are also shown in Fig. 1; a dashed line joining a group to its subgroup indicates that the corresponding phase transition is required by Landau theory to be first order.

It is interesting to re-examine the literature in light of this analysis. The proposed orthorhombic structures at room temperature in *Pmmm* on a $1 \times 1 \times 2$ cell (Yoshii, 2000) and in *Pban* on a $2^{1/2} \times 2^{1/2} \times 2$ cell (Sefat *et al.*, 2005) do not appear as possibilities in Fig. 1. The other proposal is that $Nd_{2/3}TiO_3$ is isostructural with $La_{2/3}TiO_3$ (Howard & Zhang, 2004*a*,*b*; Sefat *et al.*, 2005) in the space group *Cmmm* on a $2 \times 2 \times 2$ cell, a structure that has been shown already (Howard & Zhang, 2004*a*,*b*) to be consistent with the symmetry analysis above. This orthorhombic structure ($a^-b^0c^0$ using Glazer's notation) is characterized by *A*-site cation/vacancy ordering along the *z* axis and out-of-phase TiO_6 octahedral tilting around an axis (*x*

[1] *ISOTROPY* is a software package developed by Stokes and Hatch at Brigham Young University. *ISOTROPY* is available at http://www.physics.byu.edu/~stokesh/isotropy.html.

axis) perpendicular to the ordering direction. However, because of the slightly smaller ionic radius of Nd^{3+} (Shannon, 1976), hence the lower perovskite tolerance factor $\{t = (R_A + R_O)/ [2^{1/2}(R_B + R_O)]$, where R_A, R_B and R_O are the ionic radii of the *A*- and *B*-site ions and the O ion, respectively (Goldschmidt, 1926; Roth, 1957)$\}$, $Nd_{2/3}TiO_3$ is expected to show greater octahedral tilting than $La_{2/3}TiO_3$ and possibly lower symmetry due to tilting around more than one axis (Reaney *et al.*, 1994). In fact, our experiments did indicate that the orthorhombic structure in *Cmmm* was only observed at high temperatures for $Nd_{0.7}Ti_{0.9}Al_{0.1}O_3$, following a continuous phase transition at around 750 K (see §4). Therefore, as can be seen from Fig. 1, the only possibilities for the room-temperature structure are the structures in *C*2/*m* ($a^-b^0c^-$ on a 2 × 2 × 2 cell), *Pmma* ($a^+b^-c^0$ on a 2 × 2 × 2 cell), *Amm*2 ($a^-b^0c^+$ on a 2 × 2 × 2 cell) or *P*2/*m* ($a^-b^-c^0$ on $2^{1/2} \times 2 \times 2^{1/2}$ cell) – these are the only subgroups allowing a single, possibly continuous transition to the structure in *Cmmm*.

3. Experimental

$Nd_{0.7}Ti_{0.9}Al_{0.1}O_3$ samples were produced by our standard alkoxide/nitrate route (Ringwood *et al.*, 1988). This method involved the mixing of correct molar quantities of titanium isopropoxide and aluminium *sec*-butoxide in ethanol with aqueous solutions of neodymium nitrate, while continuously stirring. After thorough mixing and stir drying, the materials were calcined in air at 1023 K for 1 h to remove nitrates and alcohol, followed by wet milling for 16 h using zirconia balls. The slurry was then dried at 383 K overnight and the dried clumps were crushed in a mortar and pestle into fine powder. The powder was pelletized and sintered in air at 1723 K for 48 h, then furnace cooled. A polished surface was carbon-coated and characterized by scanning electron microscopy (SEM), using a Jeol 6400 instrument fitted with a Tracor Northern energy-dispersive spectrometer (EDS) operated at 15 kV. A comprehensive set of standards was used for the quantitative work, giving a high degree of accuracy. This verified the sample composition and showed the sample to be homogeneous with a very small amount of $Nd_2Ti_2O_7$ (the amount of impurity phase was below the detection limit by X-ray powder diffraction using a Philips X'Pert Pro Diffractometer with Cu $K\alpha$ radiation).

Time-of-flight neutron powder diffraction data were recorded using the high-resolution powder diffractometer, HRPD, at the ISIS neutron facility, Rutherford Appleton Laboratories, UK (Ibberson *et al.*, 1992). The temperature range of interest, from 4.2 to 1273 K, necessitated the use of both cryostat and furnace. For measurements in the cryostat at 4.2, 100 and 200 K, the powdered sample was lightly packed into an aluminium can of slab geometry, area 20 × 20 mm, 15 mm thick, with thin neutron-transparent windows front and back. Heat was supplied to the sample through a 100 W cartridge heater inserted in the side wall of the sample can and temperature was monitored using a Rh/Fe sensor located in the opposite wall. A gadolinium, neutron-absorbing mask was attached to the side of the can facing the incident and back-scattering detectors to reduce contaminant Bragg peaks arising from either the body of the sample can, including sensor or heater, or the stainless steel frames supporting the vanadium windows. The assembly was attached to a centre-stick and mounted in an AS Scientific, 50 mm diameter, 'Orange' helium cryostat, located at the 1 m position of the diffractometer. The exchange gas was He at 30 mbar. For measurements at room temperature and above, the sample was loaded into an 11 mm diameter vanadium can, which was then either suspended from the standard ISIS candlestick for room-temperature measurements or mounted in the RAL vacuum furnace for temperature runs from 373 to 1273 K in 100 K steps. The furnace

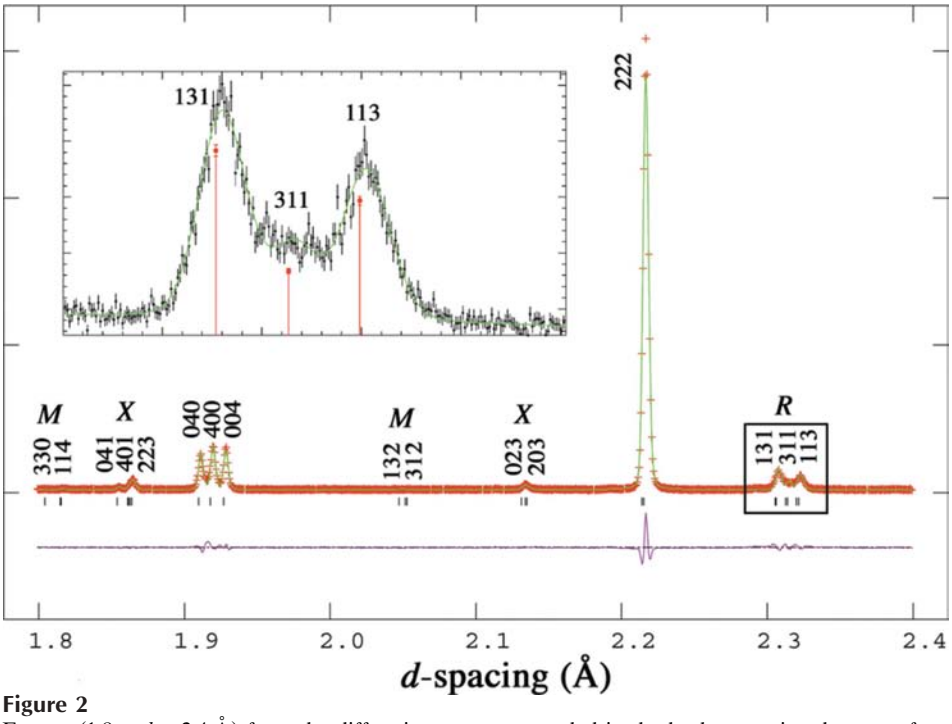

Figure 2
Extract ($1.8 < d < 2.4$ Å) from the diffraction pattern recorded in the back-scattering detectors from $Nd_{0.7}Ti_{0.9}Al_{0.1}O_3$ at room temperature. The peaks are indexed on a cell of dimensions (referred to the edge of the cubic aristotype) 2 × 2 × 2. Crosses represent the observed data. The continuous lines are fits obtained by the Rietveld method using the proposed structure in *C*2/*m*, the vertical marks show the peak positions expected in this structure and the line beneath the pattern records the difference between the observed pattern and that calculated in the Rietveld analysis. The inset shows details of the 131/311/113 reflections (boxed region). The solid line through the data points is the envelope of the Voigt/sharp-edged exponential three-peak fit and the vertical lines indicate the individual peak intensities and positions (with error bars).

Table 1
Details of the room-temperature monoclinic and high-temperature orthorhombic structures of $Nd_{0.7}Ti_{0.9}Al_{0.1}O_3$.

The Wyckoff symbol for each site is shown. The number in parentheses beside each entry indicates the s.u. referred to the last digit shown. The Nd site at $z \simeq 0$ is essentially fully occupied; the occupancy of the site at $z \simeq 1/2$ is close to 40%.

Atom	Site	x	y	z	Occupancy	U
Room temperature (296 K), space group $C2/m$, a = 7.6764 (1), b = 7.6430 (1), c = 7.7114 (1) Å, β = 90.042 (2)°						
Nd1	4(*i*)	0.2522 (6)	0	0.0022 (8)	0.970 (5)	0.91 (9)
Nd2	4(*i*)	0.2493 (14)	0	0.5096 (17)	0.430 (5)	0.97 (18)
Ti,Al	8(*j*)	0.0046 (11)	0.2474 (9)	0.2606 (5)	0.9, 0.1	0.53 (6)
O1	4(*g*)	0	0.2827 (6)	0	1	1.45 (27)
O2	4(*h*)	0	0.2231 (8)	0.5	1	3.44 (31)
O3	4(*i*)	0.0135 (7)	0	0.2092 (5)	1	1.15 (24)
O4	4(*i*)	−0.0297 (8)	0.5	0.2683 (5)	1	1.56 (27)
O5	8(*j*)	0.2536 (8)	0.2730 (7)	0.2338 (4)	1	2.49 (20)
						Measure of fit: χ^2 = 4.2
T = 873 K, space group $Cmmm$, a = 7.7102 (1), b = 7.6943 (1), c = 7.7476 (1) Å						
Nd1	4(*g*)	0.2503 (8)	0	0	0.989 (5)	2.28 (11)
Nd2	4(*h*)	0.2535 (18)	0	0.5	0.411 (5)	2.25 (21)
Ti,Al	8(*n*)	0	0.2477 (14)	0.2623 (4)	0.9, 0.1	1.64 (7)
O1	4(*i*)	0	0.2805 (8)	0	1	3.37 (31)
O2	4(*j*)	0	0.2254 (10)	0.5	1	4.28 (34)
O3	4(*k*)	0	0	0.2111 (6)	1	2.53 (32)
O4	4(*l*)	0	0.5	0.2649 (7)	1	4.46 (41)
O5	8(*m*)	0.25	0.25	0.2354 (7)	1	4.54 (23)
						Measure of fit: χ^2 = 2.3

has vanadium heating elements and the thermometry is based on type-K thermocouples positioned in contact with the sample can at about 20 mm above the beam centre. The sample temperature was controlled to ± 0.2 K. Diffraction patterns from the sample, whether in cryostat or furnace, were recorded over the time-of-flight range 30–130 ms in both back-scattering and 90° detector banks, corresponding to d-spacings from 0.6 to 2.6 Å (at a resolution of $\Delta d/d \simeq 4 \times 10^{-4}$) and from 0.9 to 3.7 Å ($\Delta d/d \simeq 2 \times 10^{-3}$), respectively. The patterns were normalized to the incident-beam spectrum as recorded in the upstream monitor and corrected for detector efficiency according to prior calibration with a vanadium scan. Patterns were recorded to a total incident proton beam of *ca* 75 μA h at room temperature and above, and 100 μA h below room temperature, corresponding to approximately 2.3 and 3.1 h of data collection, respectively, to allow good structure determinations.

4. Results and discussion

An extract from the neutron diffraction pattern, $1.8 < d < 2.4$ Å, recorded from $Nd_{0.7}Ti_{0.9}Al_{0.1}O_3$ at room temperature is shown in Fig. 2. The peaks in the figure are identified by indices based on the $2 \times 2 \times 2$ cell. Peaks with all-even indices correspond to peaks from the ideal cubic aristotype. The superlattice peaks are also indexed on the basis of the $2 \times 2 \times 2$ cell and are marked as the X point (two even, one odd indices), R point (all odd indices) or M point (one even, two odd indices). Intensities at the X points arise from A-site cation/vacancy ordering and those at the R points from out-of-phase (−) octahedral tilting. Intensities at the M points could arise from in-phase (+) octahedral tilting; alternatively, very weak intensities (as observed) could appear at these points due to X- and R-point distortions acting in concert.

The inset of Fig. 2 shows the details of the 131/311/113 R-point reflections. In order to separate the individual components, this region was fitted with three peaks each comprising a Voigt function convolved with a sharp-edged exponential, on a linear background – assuming all peaks have the same widths and shapes.[2] The heights of the three vertical lines indicate the individual peak intensities, showing that the intensities are in the order of 131 reflection > 113 reflection > 311 reflection. According to Glazer (1975), a^- (out-of-phase tilting around the x axis) produces reflections of approximately equal intensities at *odd–odd–odd* with $k \neq l$ (here 131 and 113), b^- reflections with $h \neq l$ (113 and 311) and c^- reflections with $h \neq k$ (131 and 311). Applying the above results from Glazer, we can now rule out three of the possible structures enumerated from group-theoretical analysis (Fig. 1): structures in *Amm*2 ($a^-b^0c^+$), *Pmma* ($a^+b^-c^0$) and *P*2/*m* ($a^-b^-c^0$). The structures in *Amm*2 ($a^-b^0c^+$) and *Pmma* ($a^+b^-c^0$) would not have produced any intensity at the observed 311 and 131 reflections, respectively, while the structure in *P*2/*m* ($a^-b^-c^0$) would have resulted in the 113 peak being the strongest (*not* the 131 reflection as observed). This leaves the structure in *C*2/*m* ($a^-b^0c^-$) as the only possibility. Indeed, such a structure, according to Glazer (1975), does produce the relative intensities as observed [$I(131) > I(113) > I(311)$]. The elimination of structures in *Amm*2 ($a^-b^0c^+$) and *Pmma* ($a^+b^-c^0$), both involving in-phase (+) octahedral tilting, is supported by the fact that the observed intensities of all the M-point reflections are either very weak or negligible, consistent with the origin of these superlattice peaks as the combination of A-site cation/vacancy ordering (X point) and out-of-phase (−) octahedral tilting (R point), rather than in-phase (+) octahedral tilting. Based on the above arguments, we propose the structure in

[2] Peak-fitting program due to Devinder Sivia, ISIS Facility.

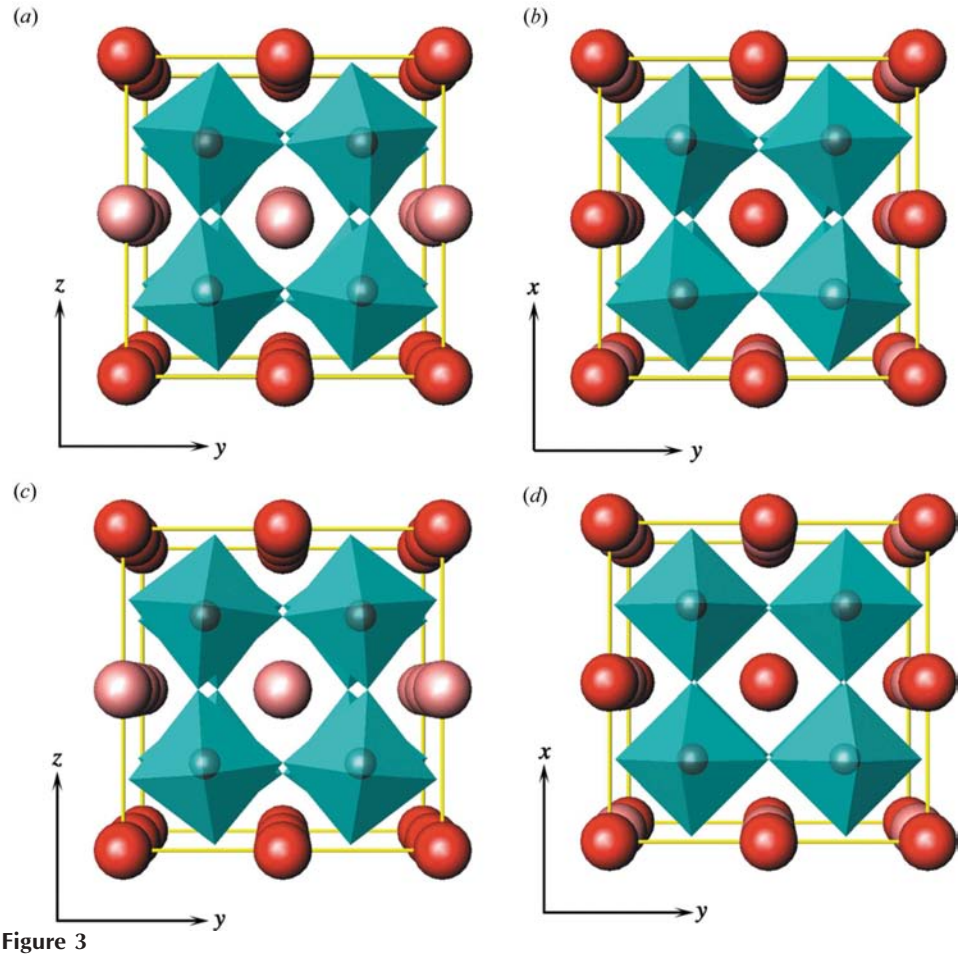

Figure 3
Representations of (*a*), (*b*) room-temperature monoclinic, and (*c*), (*d*) high-temperature orthorhombic structures of $Nd_{0.7}Ti_{0.9}Al_{0.1}O_3$. The $(Ti/Al)O_6$ groups are shown as octahedra, the Ti/Al ion being visible within them; the darker and lighter spheres outside these octahedra represent Nd in the fully and partly occupied layers, respectively. The unit cell is outlined in each case. The figures shown are perspective views along the *x* and *z* axis. The movements of O^{2-} and Ti^{4+}/Al^{3+} ions respectively towards and away from the fully occupied Nd layers result in an offset of the Ti/Al atom discernible in (*a*) and (*c*). The octahedral tilting in (*a*), (*b*) and (*c*) is also clearly visible. These figures were prepared using the computer program *ATOMS* (Dowty, 1999).

*C*2/*m*, tilt system $a^-b^0c^-$, as the room-temperature structure for $Nd_{0.7}Ti_{0.9}Al_{0.1}O_3$.

The diffraction pattern has been fitted, and both lattice parameters and atomic coordinates were determined using the Rietveld method as implemented in the *GSAS* computer program (Larson & von Dreele, 2000; Toby, 2001). Patterns from both the back-scattering and the 90° detector banks were fitted simultaneously, the diffractometer constant for the 90° bank being released to ensure that the lattice parameters were determined in every case by the higher-resolution back-scattering bank. Internal coordinates were refined along with displacement parameters and oxygen displacement parameters were taken to be anisotropic (however, in refinements of the very slightly distorted monoclinic structure, the oxygen displacement parameters were constrained to correspond to orthorhombic *Cmmm* symmetry). The isotropic displacement parameters for the two *B*-site cations, Ti^{4+} and Al^{3+}, were constrained to be equal. The distribution of the Nd^{3+} ions over the two crystallographically distinct *A* sites was allowed to vary, with the total occupancy constrained to 1.4. The details of the structure, as refined by the Rietveld method, are included in Table 1. This monoclinic structure, along with the structure of the high-temperature orthorhombic phase, is depicted in Fig. 3. Note that a refinement from the room-temperature data was also carried out assuming the *Cmmm* model; the goodness-of-fit (χ^2 = 5.0) was, as expected, worse than for the *C*2/*m* model.

As shown in Table 1,[3] the room-temperature refinement confirms the cation ordering to the extent that the *A* sites at $z \simeq 0$ are essentially fully occupied by Nd^{3+} ions (97% occupancy), while the *A* sites at $z \simeq 1/2$ contain nearly all the vacancies (43% occupancy). It can be seen, from the values of *z* tabulated, that the Ti^{4+}/Al^{3+} ions move away from the fully occupied layer and the O^{2-} ions move (on average) towards it, as might be expected given the additional positive charge on these layers. Not only do these movements make sense, but also they may well account for the stability of the layered ordering that is observed (Thomas *et al.*, 2006). The distinctive feature of the present model is the movement of O atoms associated with octahedral tilting around both the *x* and *z* axes. The angles of tilt can be estimated from the oxygen coordinates as the angle made by the line joining O3 with O4 to the *y* axis. This tilt angle around the *x* axis is given by $\tan^{-1}\{[z(O4) - z(O3)]c/(b/2)\}$ and is $\sim 6.8°$. Similarly the tilt angle around the *z* axis is given by $\tan^{-1}\{[x(O3) - x(O4)]a/(b/2)\}$ and is $\sim 5.0°$. These angles are bigger than the tilt angle of $\sim 4.7°$ (around the *x* axis only) reported for $La_{0.6}Sr_{0.1}TiO_3$ at room temperature (having an orthorhombic structure in *Cmmm*; Howard & Zhang, 2003), consistent with (see §2) the slightly smaller ionic size of Nd^{3+} compared with La^{3+}.

Diffraction patterns obtained at high temperatures were inspected closely to look for phase transition(s). In fact, this was done before the room-temperature structure was solved,

[3] Supplementary data for this paper are available from the IUCr electronic archives (Reference: BK5024). Services for accessing these data are described at the back of the journal.

since that relied upon the correct identification of the high-temperature structure and a consideration of structures derived from it (see §2). As in the case of $La_{0.6}Sr_{0.1}TiO_3$, layered ordering of cations/vacancies is expected to remain in the temperature range of this study (up to 1273 K) due to the low cation mobility (Howard & Zhang, 2003). However, phase transitions due to the disappearance of octahedral tilting are expected upon heating. Again the details of the superlattice peaks proved to be pivotal. Fig. 4(*a*) shows details of the 131/311/113 reflections observed at various temperatures. The same peak-fitting procedure, as that applied to the room-temperature data, was carried out for all the temperature runs. The results at T = 100, 673 and 773 K are shown in Figs. 4(*b*)–(*d*), respectively; the vertical lines indicate the intensity of each individual peak. For temperatures up to 673 K, three peaks are necessary to fit the 131/311/113 region satisfactorily. For temperatures ranging from 773 to 1273 K, however, the intensity of the middle 311 peak becomes negligible, *i.e.* only two peaks are required to fit this region. According to Glazer (1975), the appearance of intensity in *R*-point reflections with $k \neq l$ (*i.e.* 131 and 113), together with the absence of intensity at the corresponding $k = l$ reflection (*i.e.* 311), implies that only around the x axis does the (out-of-phase) octahedral tilt occur. This is similar to the diffraction pattern obtained at room temperature from $La_{0.6}Sr_{0.1}TiO_3$, which was successfully refined using a structure model in *Cmmm*, tilt system $a^-b^0c^0$ (Howard & Zhang, 2003). Therefore, we propose the same orthorhombic structure for the high-temperature phase of $Nd_{0.7}Ti_{0.9}Al_{0.1}O_3$.

Diffraction patterns were also recorded below room temperature at 4.2, 100 and 200 K, to check for a possible low-temperature phase. The details of the 131/311/113 reflections at 4.2, 100 and 200 K are shown in Figs. 4(*a*) and (*b*); the presence of the middle 311 peak is more evident at lower temperatures due to the slightly wider spacing between peaks. The diffraction patterns are, however, exceedingly well fitted

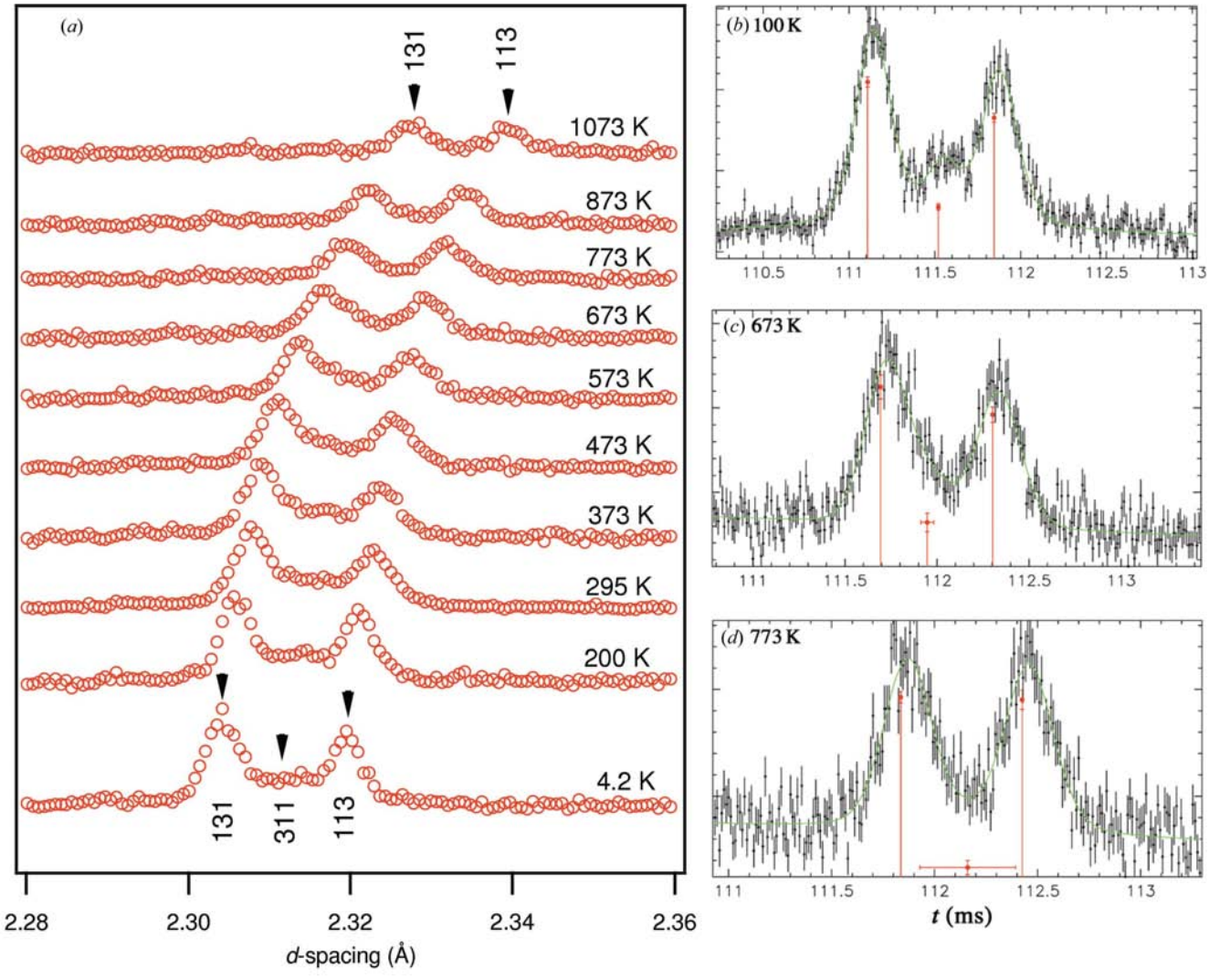

Figure 4
(*a*) Details of the 131/311/113 reflections (2.28 < d < 2.36 Å) at temperatures ranging from 4.2 to 1073 K, (*b*)–(*d*) curve-fitting results of the same region at 100, 673 and 773 K, respectively. Note the abscissae in (*b*)–(*d*) are time-of-flight, related to d-spacing by t (ms) = 48.235d (Å). The solid line through the data points in (*b*)–(*d*) is the envelope of the Voigt/sharp-edged exponential peak fits and the vertical lines indicate the individual peak intensities and positions (with error bars).

assuming the same $C2/m$ structure as occurs at room temperature, suggesting that there is no additional phase occurring below room temperature.

Structure refinements were carried out for all the temperature runs, from 4.2 to 1273 K, using the same protocol as described earlier. The results of the refinement from the patterns recorded at 873 K, a temperature at which the orthorhombic structure is well established, are also shown in Table 1. The refinements confirm the cations are still ordered in the high-temperature orthorhombic phase, such that one layer is essentially fully occupied by Nd^{3+} ions and the next contains nearly all the vacancies. As noted in the monoclinic structure at room temperature, the values of z tabulated for the orthorhombic structure at 873 K also reveal that the Ti^{4+}/Al^{3+} ions move away from the fully occupied layer, and the O^{2-} ions move (on average) towards it. The driving force for the phase transition to orthorhombic is the disappearance of the octahedral tilting around the z axis, leaving only the tilting around the x axis. Again this angle is given by $\tan^{-1}\{[z(\mathrm{O4}) - z(\mathrm{O3})]c/(b/2)\}$ and is $\sim 6.2^\circ$ at 873 K, slightly smaller than that at room temperature.

Lattice parameters obtained from the refinements are recorded in Fig. 5. The cell edges show saturation effects at lower temperatures, and accordingly have been fitted with functions of the form $l = l_0 + l_1\theta_s \coth(\theta_s/T)$ (Salje *et al.*, 1991) with saturation temperature θ_s at 350 K. At 1273 K, the highest temperature studied, the structure is still clearly orthorhombic. Extrapolating on parameters a and b suggests that a transition to a tetragonal structure might occur at around 1480 K. This would be the structure, space group $P4/mmm$, formed by perovskites with layered cation/vacancy ordering on the A sites in the absence of octahedral tilting and adopted, for example, by $La_{0.6}Sr_{0.1}TiO_3$ at elevated temperatures (Howard & Zhang, 2003). However, the possibility of other effects, such as the onset of disorder on the A site due to increased cation mobility at high temperatures, cannot be excluded.

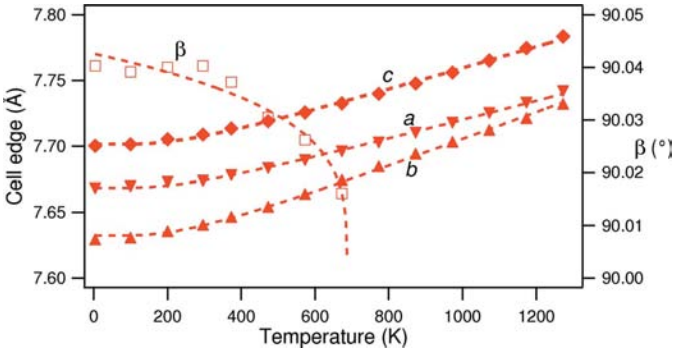

Figure 5
Lattice parameters for $Nd_{0.7}Ti_{0.9}Al_{0.1}O_3$ as a function of temperature. The dashed curves fitted to the cell edges are of the form $l = l_0 + l_1\theta_s\coth(\theta_s/T)$, with θ_s = 350 K, to describe the saturation effects at lower temperatures. Extrapolation on a and b suggests the structure would become tetragonal at around 1480 K. The curve fitted to the monoclinic angle is of the form $\beta - 90^\circ \propto (T_c - T)^{1/4}$, consistent with a tricritical transition occurring at $T_c \simeq 690$ K.

The monoclinic β angle is fitted reasonably well with a function of the form $\beta - 90^\circ \propto (T_c - T)^{1/4}$, with T_c = 690 K, consistent with a continuous but tricritical phase transition from the monoclinic to the orthorhombic phase (Salje, 1990). The continuous nature of this phase transition is confirmed by directly comparing the diffraction patterns from the monoclinic phase with those from the orthorhombic phase – there are no discernible differences aside from the subtle ones in R-point reflections already discussed. The transition temperature from monoclinic to orthorhombic cannot be determined very accurately due to the coarse (100 K) temperature steps used as well as the difficulty (see β in Fig. 5) in obtaining precise estimates of the small monoclinic distortion. Based on our observations of the R-point reflections (Fig. 4), we believe the transition occurs between 673 and 773 K, so tentatively suggest 750 K for the temperature of this transition.

Finally, it should be mentioned that our model for the room-temperature structure in $C2/m$ was used successfully to generate the selected-area electron diffraction (SAED) patterns recorded by Lee *et al.* (2004) in their TEM study of $Nd_{0.7}Ti_{0.9}Al_{0.1}O_3$. Calculated patterns were obtained using the program *EMS On Line* (Electron Microscopy Image Simulation[4]), which includes multiple scattering effects. In addition, a multiple domain effect was taken into consideration as the SAED patterns recorded by Lee *et al.* (2004) were from at least two different domains due to the small domain size in their sample. It is clear that the superlattice reflections indexed at $\frac{1}{2}(odd\ odd\ odd)$, $\frac{1}{2}(odd\ even\ even)$ and $\frac{1}{2}(odd\ odd\ even)$ in their paper (referred to the $1 \times 1 \times 1$ cubic cell of the aristotype) can be accounted for by the out-of-phase octahedral tilting, the layered ordering of the Nd^{3+} ions and a combination of the two, respectively. The manner in which 'concert' reflections can be produced by combinations of distortions is highlighted in recent simulations by Woodward & Reaney (2005). It is not necessary in the present case to invoke in-phase tilting or any particular A-site cation displacement as Lee *et al.* (2004) proposed.

5. Summary and conclusions

The room-temperature structure of $Nd_{0.7}Ti_{0.9}Al_{0.1}O_3$, which we take to represent the structure of $Nd_{2/3}TiO_3$, has been successfully determined. Symmetry arguments were used to limit the possibilities, then the structure solution completed from a high-resolution neutron powder diffraction study revealed details of the weak superlattice reflections that arise from octahedral tilting. The structure, monoclinic in $C2/m$, has been successfully refined by the Rietveld method. It is characterized by a layered ordering of the A-site cations/vacancies along the z axis (alternately occupied and partly occupied layers of Nd cations), and out-of-phase tilting of the $(Ti/Al)O_6$

[4] *EMS On Line* is an internet version of the commercial software package developed by Pierre Stadelmann at the Centre Interdépartemental de Microscopie Electronique (CIME) of the Ecole Polytechnique Fédérale de Lausanne (EPFL) in Switzerland. The interface for this version (http://cimesg1.epfl.ch/CIOL/ems.html) was developed by Pierre-Henri Jouneau.

octahedra independently around two axes (~ 6.8 and 5.0° around the x and z axes, respectively).

The phase transition to orthorhombic in *Cmmm* has also been examined, with the transition temperature roughly estimated at around 750 K. The driving force for this phase transition is the disappearance of the octahedral tilting around the z axis (parallel to the direction of the cation ordering). Upon further heating (beyond the temperature range of this experiment), the octahedral tilting around the x axis (perpendicular to the direction of the cation ordering) is also expected to disappear, leading to a tetragonal structure in *P*4/*mmm*, as observed for $La_{0.6}Sr_{0.1}TiO_3$ (Howard & Zhang, 2003).

The authors thank Mr Ian Watson, Ms Melody Carter of the Australian Nuclear Science and Technology Organisation for preparing the sample used in this study. Thanks are also due to Mr Min-Han Kim and Professor Sahn Nahm of the Korea University for their cooperation and efforts to fabricate the sample. The neutron facilities at ISIS are operated by the Council for the Central Laboratory of the Research Councils (CCLRC), with a contribution from the Australian Research Council. Travel funding to ISIS was provided by the Commonwealth of Australia under the Access to Major Research Facilities Program.

References

Dowty, E. (1999). *ATOMS*, Version 5.0.7. Shape Software, Kingsport, Tennessee 37663, USA.
Glazer, A. M. (1972). *Acta Cryst.* B**28**, 3384–3392.
Glazer, A. M. (1975). *Acta Cryst.* A**31**, 756–762.
Goldschmidt, V. M. (1926). *Strifter Norske Videnskaps – Akad. I. Mat. Naturvid. Kl.* **2**, No. 8, 1–156.
Howard, C. J. & Stokes, H. T. (2004). *Acta Cryst.* B**60**, 674–684.
Howard, C. J. & Stokes, H. T. (2005). *Acta Cryst.* A**61**, 93–111.
Howard, C. J. & Zhang, Z. (2003). *J. Phys. Condens. Matter*, **15**, 4543–4553.
Howard, C. J. & Zhang, Z. (2004*a*). *Acta Cryst.* B**60**, 249–251.
Howard, C. J. & Zhang, Z. (2004*b*). *Acta Cryst.* B**60**, 763.
Ibberson, R. M., David, W. I. F. & Knight, K. S. (1992). Rutherford Appleton Laboratory Report, RAL92-031.
Larson, A. C. & von Dreele, R. B. (2000). *GSAS*. Report LAUR 86-748. Los Alamos National Laboratory, New Mexico, USA.
Lee, H. J., Son, J. O., Oh, S. H., Cho, Y. K. & Nahm, S. (2004). *Jpn. J. Appl. Phys.* **43**, 7587–7591.
Mitchell, R. H. (2002). *Perovskites – Modern and Ancient*, ch. 5. Thunder Bay, Ontario: Almaz Press.
Reaney, I. M., Colla, E. L. & Setter, N. (1994). *Jpn. J. Appl. Phys.* **33**, 3984–3990.
Ringwood, A. E., Kesson, S. E., Reeve, K. D., Levins, D. M. & Ramm, E. J. (1988). *Radioactive Waste Forms for the Future*, edited by W. Lutze & R. C. Ewing, pp. 233–334. Amsterdam: Elsevier Science Ltd.
Roth, R. S. (1957). *J. Res. Natl. Bur. Stand.* **58**, 75–88.
Salje, E. K. H. (1990). *Phase Transitions in Ferroelastic and Co-elastic Crystals.* Cambridge University Press.
Salje, E. K. H., Wruck, B. & Thomas, H. (1991). *Z. Phys. B*, **82**, 399–404.
Sefat, A. S., Amow, G., Wu, M.-Y., Botton, G. A. & Greedan, J. E. (2005). *J. Solid State Chem.* **178**, 1008–1016.
Shannon, R. D. (1976). *Acta Cryst.* A**32**, 751–767.
Thomas, B. S., Marks, N. A. & Harrowell, P. (2006). Submitted for publication.
Toby, B. H. (2001). *J. Appl. Cryst.* **34**, 210–213.
Woodward, D. I. & Reaney, I. M. (2005). *Acta Cryst.* B**61**, 387–399.
Yoshii, K. (2000). *J. Solid State Chem.* **149**, 354–359.